Acta Geochim (2020) 39(6):811–829
https://doi.org/10.1007/s11631-020-00423-5

ORIGINAL ARTICLE

In situ LA-ICP-MS analyses of mica and wolframite from the Maoping tungsten deposit, southern Jiangxi, China

Guanghong Chen[1] · Jianfeng Gao[2] · Jianjun Lu[1] · Rongqing Zhang[1]

Received: 16 April 2020 / Revised: 4 June 2020 / Accepted: 15 July 2020 / Published online: 23 July 2020

Abstract The Maoping tungsten deposit is located in the Nanling W–Sn metallogenic belt in South China. Greisen and quartz vein types of mineralization developed in this deposit. Protolithionite occurs in the granite. Zinnwaldite is occurs mainly in greisen and wolframite–quartz veins whereas phengite is found in the underground quartz veinlets. In granite and greisen, protolithionite, and zinnwaldite are partly replaced by Li-phengite. LA-ICP-MS trace element analyses of micas and wolframite are employed to characterize the ore-forming source and evolution of ore-forming fluids. Micas show compositional variation trend in vertical directions with a decrease of W, Sn, Nb, and Ta and an increase of MgO, V, Ni, and Co. Wolframite in greisen has higher Mo, Sn, Nb, Ta, and REEs than those in quartz veins. All wolframites show similar REE patterns with enrichment of HREE. Wolframites in greisen and quartz veins have negative Eu anomalies, while wolframites in quartz veinlet display positive Eu anomalies. Compositions of mica and wolframite from different mining levels of the Maoping deposit suggest that the ore-forming fluids are dominated by magmatic hydrothermal fluids in the deep with a slight addition of meteoric water in the shallow. Brittle fracture-induced depressurization and fluid mixing controlled the evolution of ore-forming fluids and possibly lead to the wolframite deposition.

Keywords Mica · Wolframite · Magmatic-hydrothermal evolution · In situ analysis · Quartz-vein type W deposit

1 Introduction

Tungsten deposits are widely distributed in South China Block, which accounts for more than 44% of the global W reserves (Mao et al. 2019). They occur as skarn, quartz vein, porphyry, and greisen deposits (Mao et al. 2019). Among them, quartz vein-type tungsten deposits, characterized by a high grade of wolframite, are the most important tungsten sources of the world (Li et al. 2018). The quartz vein-type tungsten deposits are related to granite and are mostly distributed in southern Jiangxi, China. Previous studies have shown that both metals and ore-forming fluids are mainly originated from highly evolved granitic magmas (Mao et al. 2019 and reference therein). However, the evolutionary histories of ore-forming fluids and the process of tungsten mineralization are still not well documented.

Mica is one of the most common rock-forming minerals in granite and wolframite–quartz vein, whereas wolframite is an important tungsten mineral with hydro greisen thermal origins. At the deposit scale, the highest tungsten grades are commonly associated with mica selvages growing into the veins (Jiang 2004; Lecumberri-Sanchez et al. 2017). Micas can accommodate relatively high contents of trace elements due to the layered crystal structure. Therefore, the trace element compositions are easy to be changed with the variations of external conditions and system chemical conditions (Breiter et al. 2019; Legros

✉ Jianfeng Gao
gaojianfeng@mail.gyig.ac.cn

[1] State Key Laboratory for Mineral Deposits Research, School of Earth Sciences and Engineering, Nanjing University, Nanjing 210023, China

[2] State Key Laboratory of Ore Deposit Geochemistry, Institute of Geochemistry, Chinese Academy of Sciences, Guiyang 550081, China

et al. 2016, 2018; Li et al. 2013; Selby and Creaser 2005; Tischendorf et al. 1997). Wolframite is composed of iron and manganese tungstates. Both iron and tungsten have different valence states so that wolframite can record the geochemical composition of the ore-forming melts and fluids as well as the physico-chemical processes during its precipitate (Harlaux et al. 2018; Zhang et al. 2018). Therefore, micas and wolframite can be used to constrain the evolution processes of granitic systems, including their magmatic-hydrothermal evolution and the concomitant migration and enrichment of ore-forming elements (Breiter et al. 2019; Goldmann et al. 2013; Tindle and Breaks 2000; Xie et al. 2018).

The Maoping tungsten deposit, discovered in the 1980s, is one of the largest tungsten deposits in China. The Maoping deposit develops greisen types orebodies in the deep and wolframite–quartz vein types orebodies in the shallow. The WO_3 and Sn reserves for wolframite–quartz vein orebodies are 63,000 and 15,000 t, respectively, with average grades of 0.97% WO_3 and 0.30% Sn. Greisen orebodies host 40,000 t WO_3 and 35,000 t Sn with average grades of 0.18% WO_3 and 0.23% Sn (Hu et al. 2011a). Previous studies have carried on the basic geological characteristics of the Maoping deposit (Huang 1999; Li and Yang 1991), petrology geochemistry of ore-related granites (Zhu et al. 2012), age of granite and tungsten mineralization (Feng et al. 2011), temperature and salinity of ore-forming fluids (Chen et al. 2018; Hu et al. 2011a) and compositional variation of micas (Legros et al. 2016; Tang et al. 2016). Both mica and wolframite are well developed in greisen and wolframite–quartz veins in Maoping, providing a good opportunity to constrain the evolution history of ore-forming fluids by characterizing the vertical variation of mineral compositions.

In this paper, we describe field geology and ore petrography of the Maoping deposit and report in situ analyses of micas and wolframites from different levels at the deposit. A new dataset is used to constrain the evolution of ore-forming fluids and the variation of physico-chemical conditions of magma-hydrothermal system. We demonstrate that ore-forming fluids were mainly magmatic hydrothermal with limited addition of recycled meteoric water in the shallow level. We also discuss the role of the fracture system in the precipitation of wolframite through the comparisons of the composition of mica and wolframite from different levels.

2 Geological setting

The South China Block consists of the Yangtze Block to the northwest and the Cathaysia Block to the southeast (Fig. 1). The amalgamation of Yangtze and Cathaysia blocks along the Jiangshan-Shaoxing Fault is at 1.1–0.83 Ga (Chen and Jahn 1998; Li et al. 2007; Shui 1988; Wang et al. 2007; Xia et al. 2018; Zhao et al. 2011). The Cathaysia Block underwent extensively reworking during Caledonian, Indosinian to Yanshanian tectonic-thermal events (Yuan et al. 2018).

The Cathaysia Block is mainly composed of metamorphic basement of Precambrian–Ordovician lower greenschist facies clastic rocks and a cover of Devonian–Permian shallow marine carbonate and siliclastic sedimentary rocks. Jurassic-Quaternary terrigenous red-bed sandstones and volcaniclastics series are exposed in the region (Feng et al. 2011; Yuan et al. 2018). Silurian and Triassic strata are lacked in the region.

Mafic to felsic pluton and volcanic rocks with ages from Neoproterozoic to Cenozoic are widely distributed in the Cathaysia Block. Most plutons and volcanic rocks range are 190–80 Ma due to the subduction of the Paleo-Pacific Plate underneath the South China Block (Zhou and Li 2000; Zhou et al. 2006). Most of the tungsten and tin deposits are spatially and genetically associated with highly evolved Mesozoic granitic rocks (Mao et al. 2019 and reference therein).

The Nanling Range is in the central part of the Cathaysia Block (Fig. 1). There are several mainly regional faults closely related to the evolution of the Nanling Range, including the Pingxiang–Guilin, Longyan–Haifeng, Ganjiang–Sihui–Wuchuan faults. These regional faults control the distribution, scale, and occurrence of Mesozoic and Cenozoic igneous rocks and sedimentary basins (Shu et al. 2006). The Nanling Range hosts 8 large deposits, 24 medium deposits, and 46 small deposits (Fig. 2), among which a total reserve of WO_3 is 1.7 Mt in southern Jiangxi Province (Zeng et al. 2007). Most tungsten deposits in southern Jiangxi province are quartz-vein type (Wei et al. 2012). The majority of the large- and medium-sized ore deposits or occurrences are distributed in four ore clusters (Chongyi–Dayu–Shangyou, Ganxian–Yudu, Sannan (Longnan–Dingnan–Quannan) and Xingguo–Ningdu) (Fig. 2) (Feng et al. 2011). The Maoping deposit is located in the Chongyi–Dayu–Shangyou ore cluster.

3 Deposit geology

In the Maoping mining district, the dominant strata are the Middle and Lower Cambrian metamorphosed sandstone and slate (Figs. 3, 4). Tungsten mineralization at the Maoping deposit is mainly controlled by folds and faults. The fold structures include the Upper and Lower Maoping homoclines and the Shenfuxi–Gaoqiaoxia anticline (Fig. 3). The ore-controlling faults mainly strike E–W and dip S or N at 50°–75°. Two post-mineralization fracture

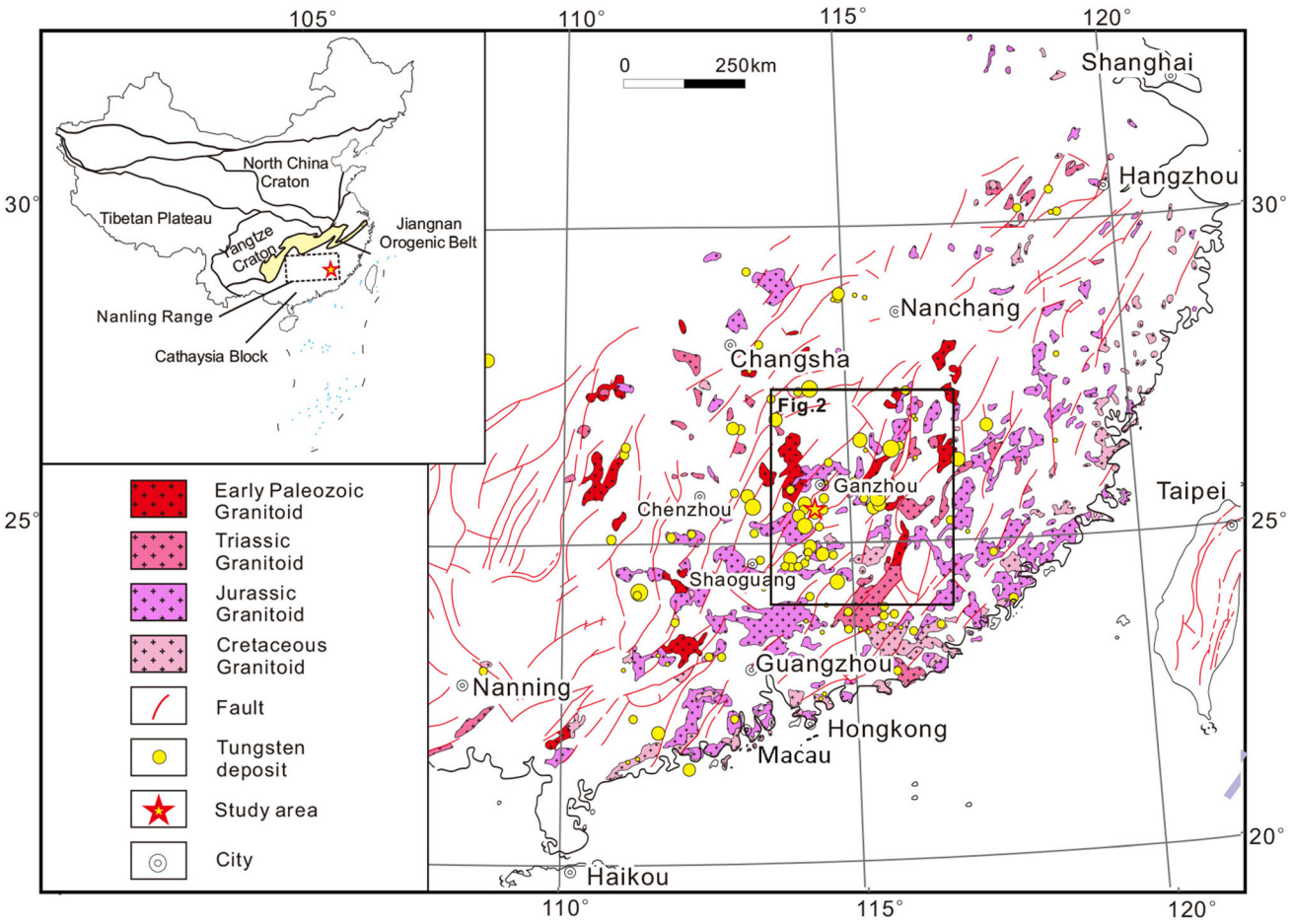

Fig. 1 Distribution and mineralization type of major tungsten deposits in South China (modified after Mao et al. 2013)

zones strike NE and NW along reverse faults (Fig. 3) (Li and Yang 1991). According to the distribution and occurrence of the ore veins, the Maoping deposit could be subdivided into three segments: Xiamaoping, Shangmaoping, and Gaoqiaoxia segments from north to south (Figs. 3, 4).

The Maoping deposit is located to the north of the Middle Jurassic Tianmenshan peraluminous granite intrusion. A buried granitic pluton, the extension of the Tianmenshan granite, is associated with the wolframite–quartz veins in the mining area (Huang 1999). The buried pluton includes porphyritic biotite granite and fine-grained muscovite granite. SHRIMP U–Pb dating on zircon show that the porphyritic biotite granite was emplaced at 151.8 ± 2.9 Ma (Feng et al. 2011).

The mineralization types at the Maoping deposit are dominated by wolframite–quartz vein type and greisen-type (Fig. 4). There are more than 400 wolframite–quartz veins which are commonly 300–500 m long and 5–100 cm thick. The vein groups of three segments all intersect in the top of the buried granite pluton, the greisen-type orebodies, pegmatite shell, and metamorphic rocks in the exocontact (Fig. 5a, b). There is a layer of pegmatite shell at the junction between the top of granite and slate. The pegmatite shell is mainly composed of quartz and mica, which is spider-like or serrated (Fig. 5c). Ore minerals in quartz-vein (Fig. 5d) and quartz-veinlets (Fig. 5e) include wolframite, cassiterite, molybdenite, sphalerite, chalcopyrite, bismuth, native bismuth, while gangue minerals are mainly quartz, mica, fluorite, and topaz.

The greisen type orebodies have a layer-like form and range from the top of the buried granite intrusion which is at − 5 m down to − 200 m. Ore minerals in greisen are mainly wolframite, cassiterite, molybdenite, bismuth, uraninite, and xenotime, whereas gangue minerals include quartz, mica, albite, and fluorite.

4 Mineralogy

4.1 Mica

Micas from granite are mainly subhedral protolithionite (Fig. 6a, b). The protolithionite is partly altered by Li-phengite (Fig. 6b). Micas of greisen consist of zinnwaldite

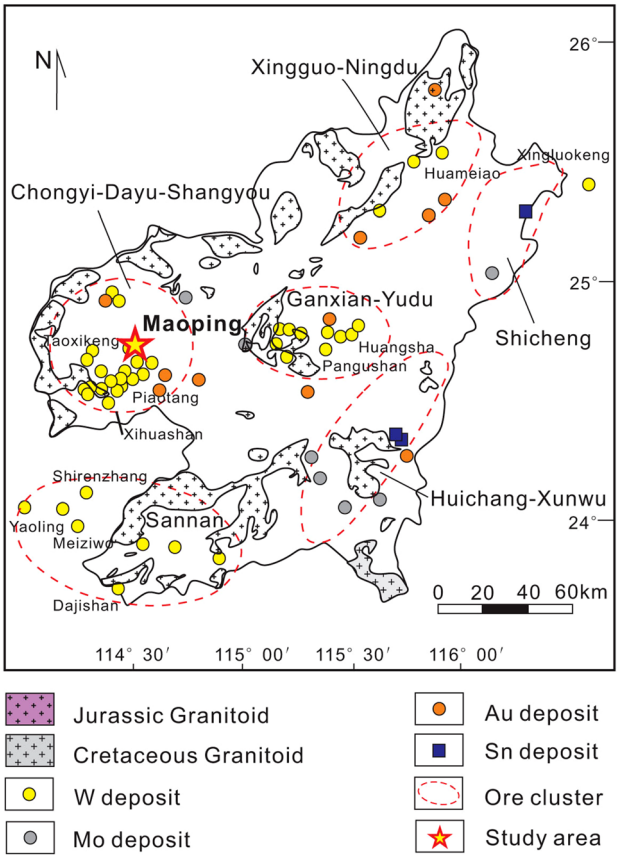

Fig. 2 Distribution of major tungsten deposits and granites in southern Jiangxi Province (modified after Huang et al. 2014)

and Li-phengite (Fig. 6c, d), which are alteration products of the granite. The mica shell in wolframite–quartz veins is dominant by zinnwaldite (Fig. 6e, f), which are metasomatic and altered by Li-phengite along the rim and fractures (Fig. 6f). The width of zinnwaldite shell is from 0.1 to 10 cm. In the shallow part of the quartz veins, mica is small with a width of mica shell in the veinlets of the ground surface of 0.1–0.3 cm.

There are two types of micas in quartz veinlets according to the BSE image under SEM. The mica with the dark domain is close to the metamorphosed sandstone, while the mica with the light domain is associated with quartz. Some mica in the veinlets has experienced chloritization.

4.2 Wolframite

The wolframite of the Maoping deposit could be classified into two types according to the occurrence of mineralization type: greisen (Fig. 7a, b) and wolframite–quartz vein (Fig. 7c–f). Wolframite grains in greisen is enhedral to subhedral with grain sizes < 100 μm. Some wolframite grains in greisen display distinct cathode luminescence domains under SEM (Fig. 7b): the inner dark domain and the outer light domain. In some grains, the light domain form rim overgrowth of the inner dark domain. Wolframite in quartz veins is bigger (up to several cm) than that in greisen. Most wolframite grains show homogeneous texture under the microscope and SEM (Fig. 7d, f).

5 Sampling and analytical methods

5.1 Sampling

Coexisting micas and wolframite were collected at different levels of mines which include the veinlet at ground surface (309 m), quartz veins of 40, − 5, − 30, − 52, − 75, − 100 m level, granite and greisen. The samples of wolframite–quartz veinlets and veins are hosted in sandstone or slate. The sampled fine-grained biotite granite has undergone a little greisenization was picked from drill hole rang from − 29.7 to − 40.1 m (drill hole: ZK30015).

5.2 Analytical methods

Back-scattered electron (BSE) images of mica and wolframite were taken with a Carl Zeiss Supra 55 field-emission scanning electron microscope (FE-SEM) coupled to a GATAN MonoCL4 detector at the State Key Laboratory for Mineral Deposits Research in Nanjing University, China. The analysis conditions were an accelerating voltage of 15 kV, a working distance of 8.5 mm, and an aperture size of 60 μm.

Quantitative chemical analyses of wolframite and micas were obtained on polished thin sections using a JEOL JXA-8100M electron microprobe (EMPA) at the State Key Laboratory for Mineral Deposits Research at Nanjing University, China. The operating conditions were set at a probe current of 20 nA, an acceleration voltage of 15 kV for all elements, and a beam diameter of 10 μm for micas and 1 μm for wolframite. The precisions of the analyses are better than 5% for major elemental (> 1 wt%).

In situ analyses of wolframite and micas in thin sections were conducted by LA-ICP-MS at Nanjing FocuMS Technology Co. Ltd. Cetac Photon Machines Analyte Excite 193 nm laser-ablation system (Bozeman, Montana, USA) and Agilent Technologies 7700 × quadrupole ICP-MS (Hachioji, Tokyo, Japan) were combined for the experiment. The 193 nm ArF excimer laser, homogenized by a set of beam delivery systems, was focused on wolframite and micas surface with a fluence of 6.0 J/cm^2. Ablation protocol employed a spot diameter of 40 μm at a 7 Hz repetition rate for 40 s. Helium was applied as a carrier gas to efficiently transport aerosol to ICP-MS. 47 elements were measured by ^{7}Li, ^{25}Mg, ^{27}Al, ^{29}Si, ^{44}Ca,

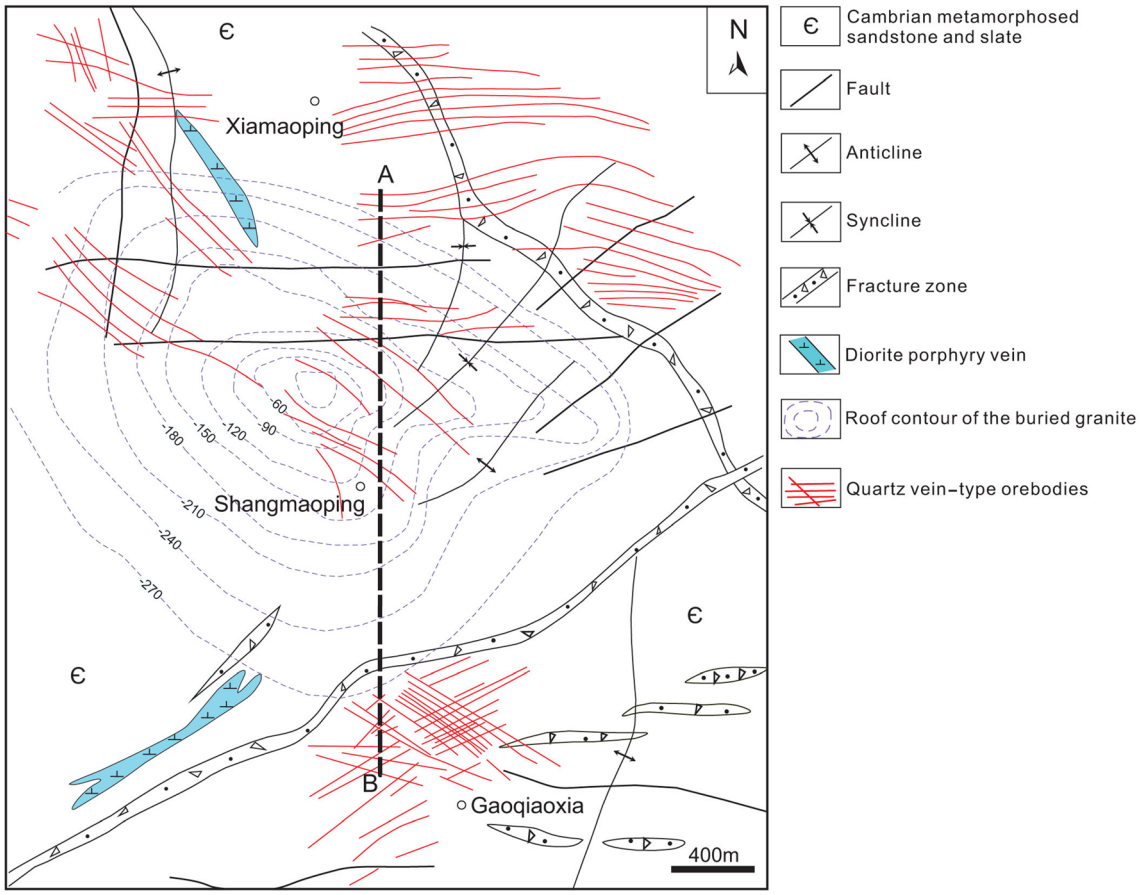

Fig. 3 Schematic geological map of the Maoping tungsten deposit (modified after Chen et al. 2018; No. 2 team of Jiangxi Nonferrous Geological Prospecting 1989)

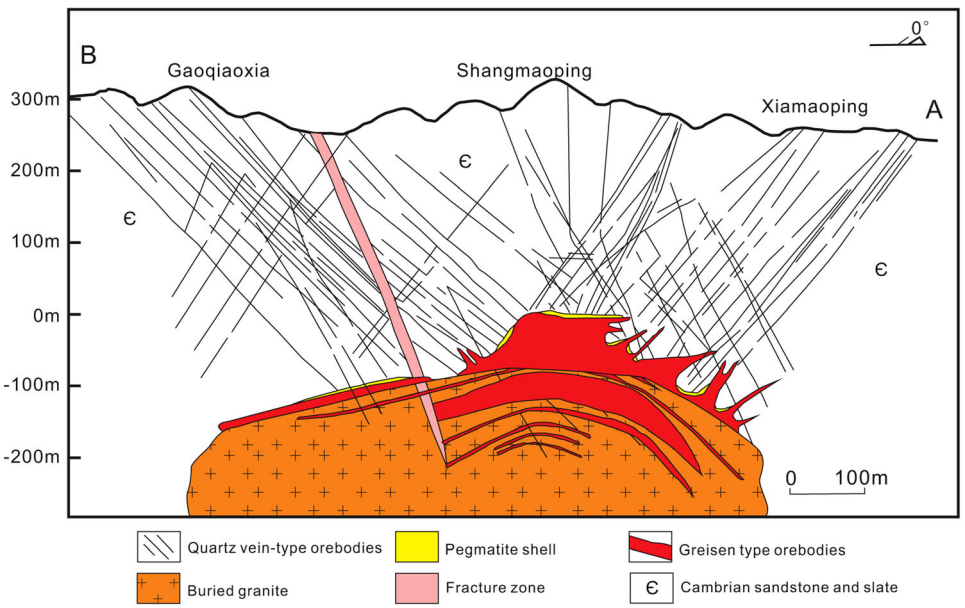

Fig. 4 Cross section of the Maoping tungsten deposit (**a**, **b** in Fig. 3) (modified after Chen et al. 2018)

^{45}Sc, ^{49}Ti, ^{51}V, ^{53}Cr, ^{55}Mn, ^{57}Fe, ^{59}Co, ^{60}Ni, ^{85}Rb, ^{88}Sr, ^{89}Y, ^{90}Zr, ^{93}Nb, ^{95}Mo, ^{118}Sn, ^{133}Cs, ^{137}Ba, ^{139}La, ^{140}Ce, ^{141}Pr, ^{146}Nd, ^{147}Sm, ^{151}Eu, ^{155}Gd, ^{159}Tb, ^{163}Dy, ^{165}Ho, ^{167}Er, ^{169}Tm, ^{173}Yb, ^{175}Lu, ^{178}Hf, ^{181}Ta, ^{182}W, ^{208}Pb, ^{232}Th and ^{238}U. United States Geological Survey basaltic glasses, including BIR-1G, BHVO-2G, BCR-2G, and GSE-

1G, were used as external calibration standards as these are of a similar matrix as anhydrous silicate (Gao et al. 2013). Raw data reduction was performed off-line by ICPMS-DataCal software using a 100 %-normalization strategy without applying internal standard (Liu et al. 2008). Chinese Geological Standard Glasses CGSG-1, CGSG-2, CGSG-4, CGSG-5 (prepared by the National Research Center for Geoanalysis, Beijing, China) were treated as quality control (Hu et al. 2011b). Analytical precision is estimated to be better than 10% of the replication of standard materials.

Fig. 6 **a** Microphotograph of protolithionite in granite, **b** BSE images ▶ showing that protolithionite in granite was replaced by Li phengite, **c** photograph of zinnwaldite in greisen, **d** BSE image showing that zinnwaldite in greisen was altered to Li phengite, **e** microphotograph of zinnwaldite in veins at − 75 m level, **f** BSE images of zinnwaldite in quartz vein, rim and fracture of zinnwaldite has been replaced by Li phengite, **g** microphotograph of phengite in veinlet (309 m), **h** BSE image showing the spatial relationship of Fe-poor phengite and Fe rich phengite (309 m). Mineral abbreviations: *Li Ph* Li phengite, *Wf* wolframite, *Znw* zinnwaldite, *Qtz* quartz, *Pl* plagioclase

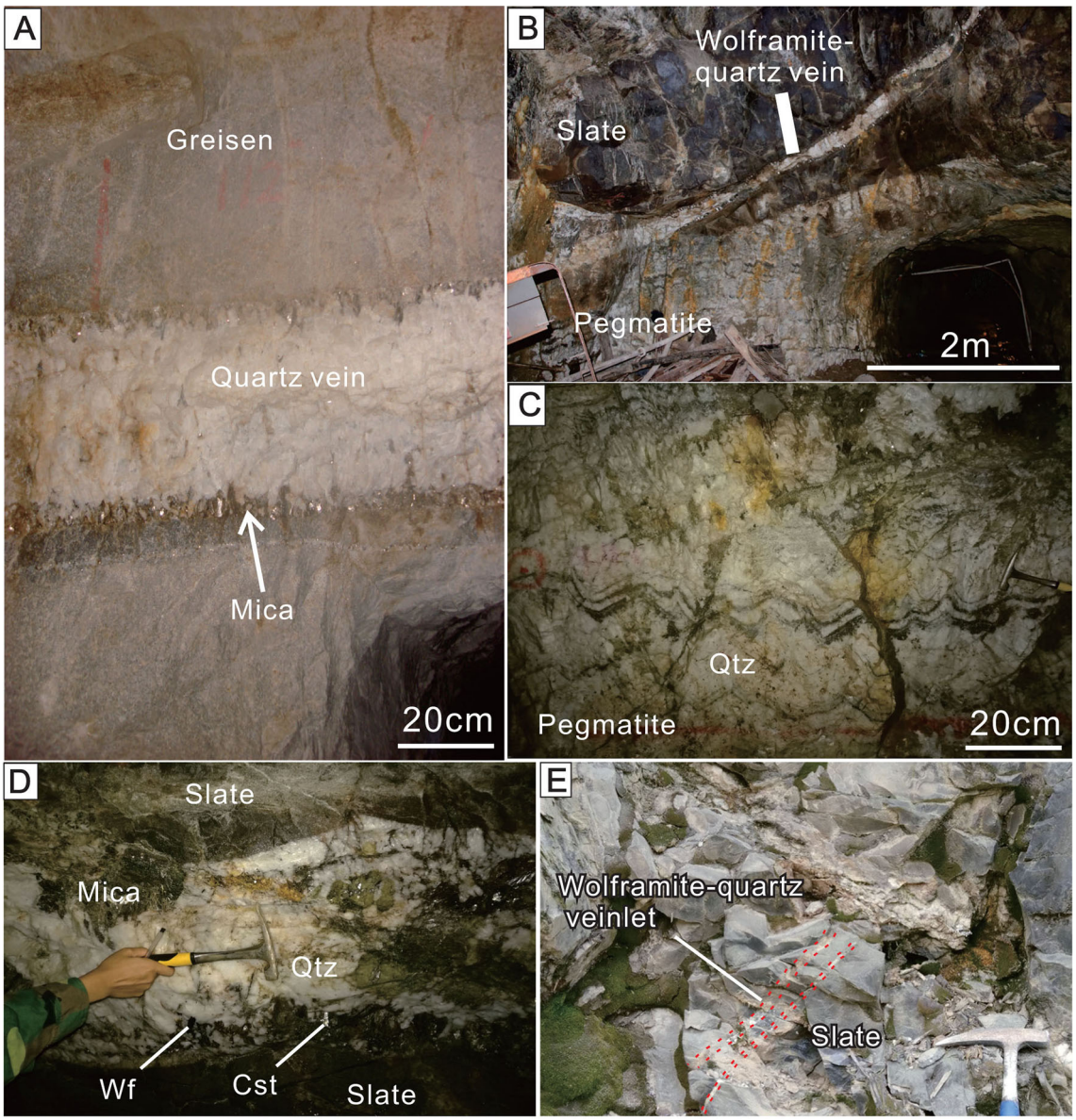

Fig. 5 **a** Wolframite quartz vein cut greisen, **b** contact relationship of wolframite quartz vein, pegmatite shell and slate, **c** The mica and quartz of pegmatite is spider-like, **d** wolframite–quartz vein (40 m) showing the occurrence of mica shell, and disseminated wolframite and cassiterite, **e** wolframite–quartz veinlet in the ground (309 m); mineral abbreviations: *Wf* wolframite, *Cst* cassiterite, *Qtz* quartz

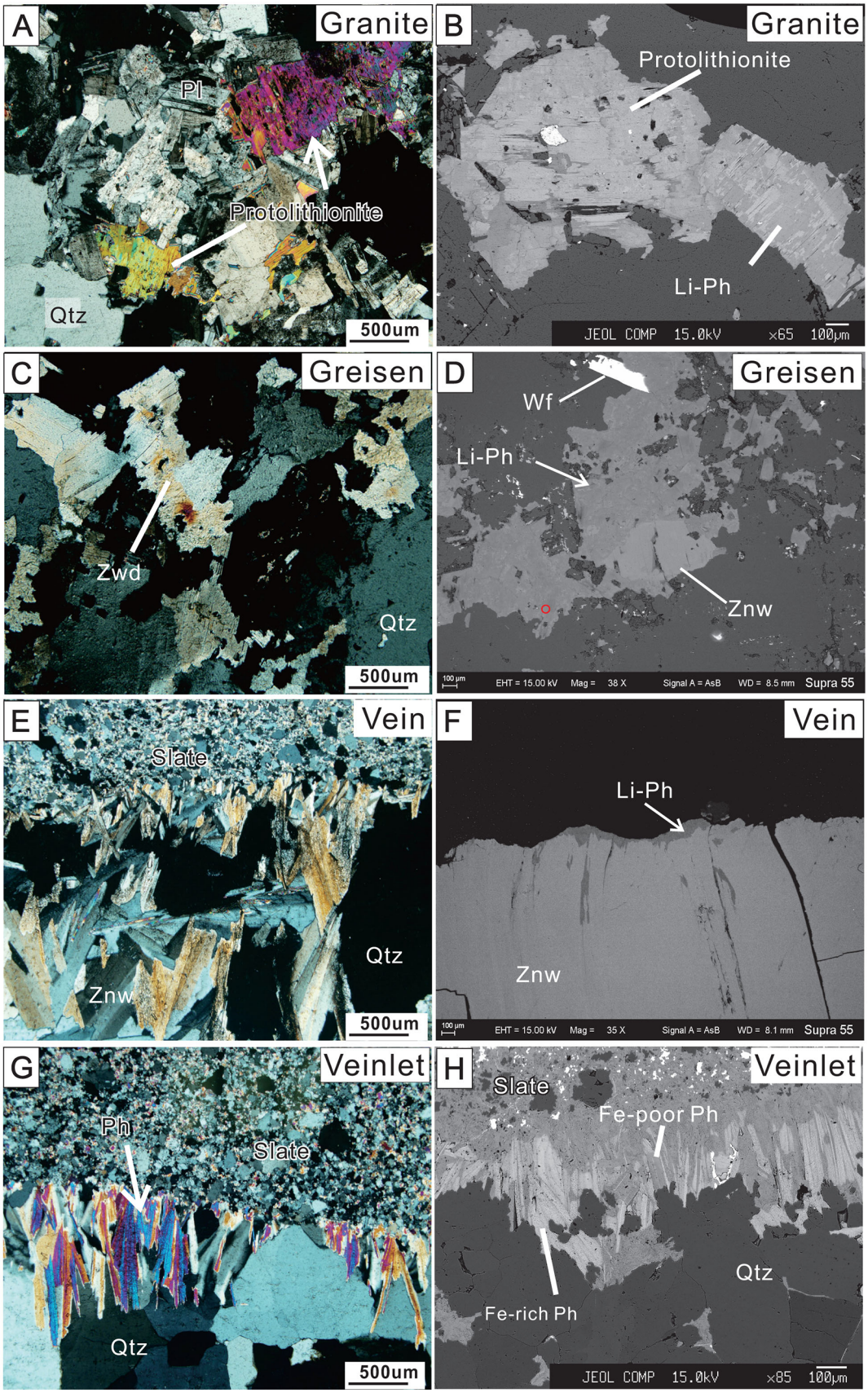
A
Granite
Pl
Protolithionite
Qtz
500um
B
Granite
Protolithionite
Li-Ph
JEOL COMP 15.0kV ×65 100μm
C
Greisen
Zwd
Qtz
500um
D
Greisen
Wf
Li-Ph
Znw
EHT = 15.00 kV Mag = 38 X Signal A = AsB WD = 8.5 mm Supra 55
E
Vein
Slate
Qtz
Znw
500um
F
Vein
Li-Ph
Znw
EHT = 15.00 kV Mag = 35 X Signal A = AsB WD = 8.1 mm Supra 55
G
Veinlet
Ph
Slate
Qtz
500um
H
Veinlet
Slate
Fe-poor Ph
Qtz
Fe-rich Ph
JEOL COMP 15.0kV ×85 100μm

The Li_2O contents can be tested accurately by LA-ICP-MS. The Li_2O contents were also estimated using SiO_2 regression for the dominantly trioctahedral micas ($Li_2O = 0.287 \times SiO_2$-9.552) and F regression for the dominantly dioctahedral micas ($Li_2O = 0.31134 \times$ F-0.075895) according to the empirical methods proposed by Monier and Robert (1986) and Tischendorf et al. (1997). A good positive linear correlation exists between Li determined by LA-ICP-MS and F or SiO_2 determined by EMPA for micas.

6 Results

6.1 Mica

Major and trace element compositions of micas from different levels are summarized in Tables 1 and 2, respectively.

Micas of the Maoping deposit can be classified into four types according to the geological occurrence, texture, and chemical composition (Fig. 8) (c.f. Tischendorf et al. 1997). The micas of granite from Legros et al. (2016) are plotted in protolithionite field while micas from granite in this study include Li-phengite and protolithionite. Micas in greisen are mainly zinnwaldite with alteration products of Li-phengite, whereas micas in wolframite–quartz veins are zinnwaldite. Micas in the veinlet of ground are plotted in phengite domain, which could be subdivided into two subtypes, including Fe-poor phengite and Fe-rich phengite.

Micas in granite, including protolithionite and Li-phengite, have relatively high F, Li, W, Sn, Nb, Ta, Sc and relatively low Mo, Co, Ni, and V (Tables 1, 2). Fluorine contents of protolithionite (average = 4.12 wt%) are higher than those of Li-phengite (average = 2.98 wt%) (Table 1; Fig. 9). Micas in greisen have a relatively high F, Li, W, Sn, Nb, Ta, and relatively low Co, Ni, Ti, V, and Sc. The Li-phengite is richer in W but poorer in Li, Nb, and Ta than the zinnwaldite (Fig. 9). Fluorine contents of zinnwaldite (average of 6.32 wt%) are higher than the Li-phengite (average of 3.92 wt%). The zinnwaldite of wolframite–quartz vein (from 40 to − 100 m) has a relatively high content of FeO, MnO, MgO, Li_2O, Sn, Nb, Ta, Mo, Co, Ni, V, and Sc. The F content of zinnwaldite range from 4.87 to

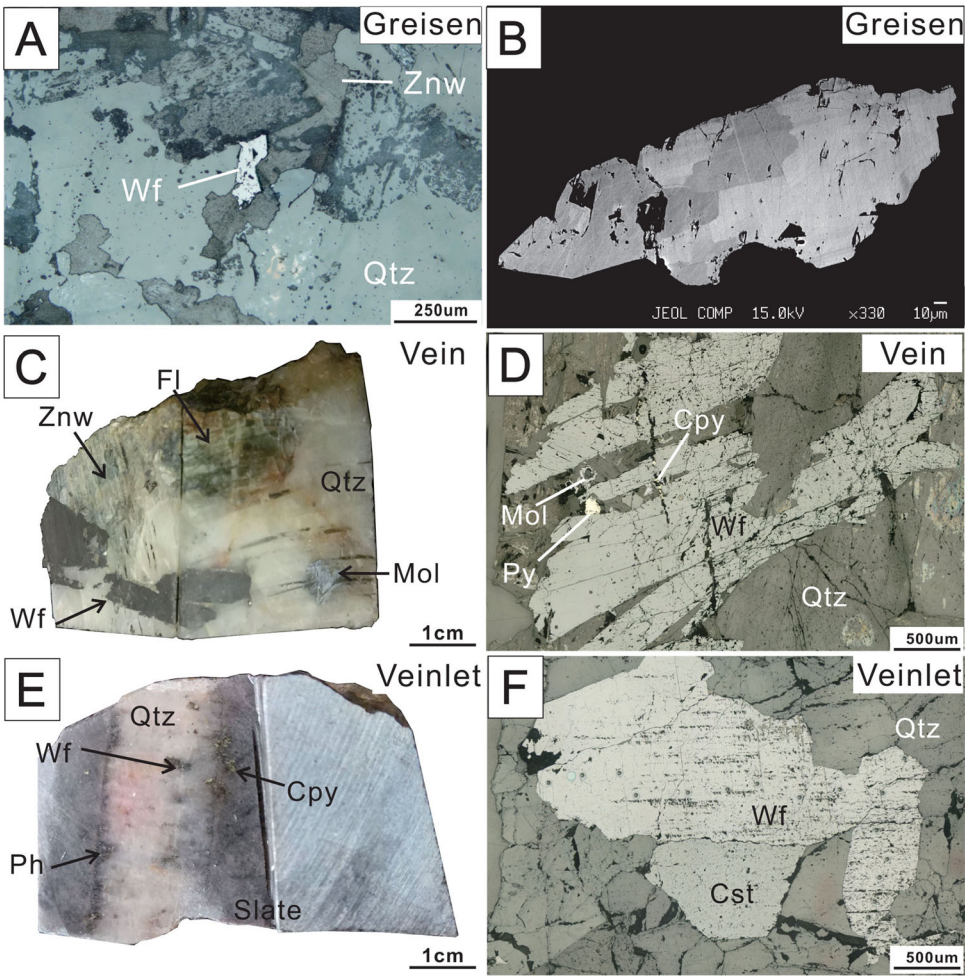

Fig. 7 **a** Microphotograph of wolframite in greisen, **b** backscattered electron images of wolframite showing the overgrowth of light domain around the inner dark domain, **c** photograph of wolframite–quartz vein (− 30 m), **d** microphotograph of mineral association of wolframite–quartz vein (− 30 m), **e** photograph of wolframite of wolframite–quartz veinlet (309 m), **f** microphotograph of wolframite of wolframite–quartz veinlet (309 m). Mineral abbreviations: *Wf* wolframite, *Cst* cassiterite, *Mol* molybdenite, *Py* pyrite, *Cpy* chalcopyrite, *Fl* fluorite, *Znw* zinnwaldite, *Qtz* quartz

Table 1 Summary of EMPA analyses of micas from the Maoping deposit

	309 m		40 m	− 5 m	− 30 m	− 52 m	− 75 m	− 100 m	Greisen		Granite	
	Fe-rich phengite Mean (n = 11)	Fe-poor phengite Mean (n = 7)	Zinnwaldite Mean (n = 15)	Zinnwaldite Mean (n = 13)	Zinnwaldite Mean (n = 5)	Zinnwaldite Mean (n = 7)	Zinnwaldite Mean (n = 39)	Zinnwaldite Mean (n = 9)	Zinnwaldite Mean (n = 7)	Li phengite Mean (n = 11)	Protolithionite Mean (n = 5)	Li phengite Mean (n = 17)
SiO_2	46.6	48.7	42.4	43.4	42.8	43.6	43.7	43.2	41.7	46.1	43.2	45.4
TiO_2	0.03	0.01	0.12	0.01	0.01	0.02	0	0.02	0.05	0.02	0.2	0.05
Al_2O_3	21.3	28.5	23.0	22.8	23.2	22.8	22.6	22.9	25.0	31.6	24.4	26.9
FeO	9.44	3.79	12.7	11.6	11.4	11.2	11.6	11.6	12.7	6.59	12.7	9.01
MnO	0.65	0.18	2.64	3.63	4	3.71	3.74	3.66	2.77	1.41	2.09	1.45
MgO	4.8	2.58	1.18	0.36	0.02	0.25	0.2	0.33	0.03	0.02	0.11	0.09
CaO	0.02	0.02	0.01	0.01	0	–	0	0	0	0.01	0.01	0.01
Na_2O	0.15	0.38	0.21	0.19	0.27	0.22	0.19	0.26	0.12	0.21	0.22	0.3
K_2O	9.7	10.1	9.82	9.91	9.7	9.94	9.42	9.82	9.73	9.87	9.77	10.1
F	5.44	3.04	6.04	6.14	6.35	6.48	6.46	6.27	6.32	3.92	4.12	2.98
Li_2O^a	1.62	0.87	2.61	2.89	2.73	2.96	2.83	2.85	2.41	1.14	1.21	0.85
H_2O^a	1.68	3.02	1.28	1.25	1.12	1.1	1.09	1.18	1.14	2.6	2.25	2.83
O = F, Cl	2.29	1.28	2.54	2.59	2.67	2.73	2.72	2.64	2.66	1.65	1.74	1.26
Total	99.2	99.8	99.4	99.5	98.8	99.6	99.0	99.5	99.3	101.8	100.1	98.7
Si(apfu)	6.57	6.55	6.13	6.25	6.22	6.27	6.31	6.23	6.04	6.2	6.15	6.41
Al^{iv}	1.43	1.45	1.87	1.75	1.78	1.73	1.69	1.77	1.96	1.8	1.85	1.59
Al^{vi}	2.1	3.07	2.06	2.12	2.18	2.14	2.15	2.13	2.31	3.2	2.24	2.88
Ti	0	0	0.01	0	0	0	0	0	0.01	0	0.02	0.01
Fe^T	1.11	0.43	1.54	1.39	1.38	1.35	1.4	1.4	1.54	0.74	1.51	1.07
Fe^{3+}	0.31	0.07	0.18	0.18	0.17	0.18	0.21	0.17	0.19	0.1	0.21	0.16
Fe^{2+}	0.8	0.36	1.36	1.21	1.21	1.17	1.19	1.23	1.34	0.62	1.32	0.9
Mn	0.08	0.02	0.32	0.44	0.49	0.45	0.46	0.45	0.34	0.16	0.25	0.17
Mg	1.01	0.52	0.25	0.08	0	0.05	0.04	0.07	0.01	0	0.02	0.02
Li^a	0.92	0.47	1.52	1.67	1.6	1.71	1.65	1.65	1.4	0.62	1.63	0.48
Ca	0	0	0	0	0	–	0	0	0	0	0	0
Na	0.04	0.1	0.06	0.05	0.08	0.06	0.05	0.07	0.03	0.05	0.06	0.08
K	1.74	1.73	1.81	1.82	1.8	1.82	1.74	1.81	1.8	1.69	1.78	1.83
OH^a	1.58	2.71	1.23	1.2	1.08	1.05	1.04	1.14	1.1	2.33	2.14	2.67
F	2.42	1.29	2.77	2.8	2.92	2.95	2.96	2.86	2.9	1.67	1.86	1.33
Y total	5.22	4.51	5.71	5.71	5.66	5.71	5.7	5.7	5.6	4.73	5.68	4.63
X total	1.79	1.83	1.87	1.88	1.87	1.88	1.79	1.88	1.83	1.75	1.84	1.91
Al total	3.53	4.52	3.93	3.87	3.97	3.87	3.84	3.9	4.27	5	4.09	4.47

Table 1 continued

	309 m		40 m	− 5 m	− 30 m	− 52 m	− 75 m	− 100 m	Greisen		Granite	
	Fe-rich phengite Mean (n = 11)	Fe-poor phengite Mean (n = 7)	Zinnwaldite Mean (n = 15)	Zinnwaldite Mean (n = 13)	Zinnwaldite Mean (n = 5)	Zinnwaldite Mean (n = 7)	Zinnwaldite Mean (n = 39)	Zinnwaldite Mean (n = 9)	Zinnwaldite Mean (n = 7)	Li phengite Mean (n = 11)	Protolithionite Mean (n = 5)	Li phengite Mean (n = 17)
$Fe^{3+}/Fe^{2+}+Fe^{3+}$	0.28	0.16	0.11	0.13	0.12	0.13	0.15	0.12	0.12	0.15	0.14	0.15

–, below detection limits

[a]Li_2O and H_2O calculation are after Tindle and Webb (1990) and Monier and Robert (1986)

7.25 wt% with an average of 6.37 wt%. The phengite in wolframite–quartz veinlet in the ground (309 m) has relatively high contents of MgO, Co, Ni, Ti, V, and relatively low contents of FeO, MnO, Li_2O, W, Sn, Nb, Ta, Mo, Sc and Zn. The Fe-rich phengite is richer in FeO, MgO, and Li_2O than the Fe-poor phengite. The F content of Fe-poor phengite (average 3.04 wt%) is lower than the Fe-rich phengite (average 5.44 wt%).

Fluorine content of protolithionite in granite and zinnwaldite in greisen and quartz-veins are higher than that of Li-phengite. Fluorine content of zinnwaldite in quartz-veins is similar to that in greisen, but higher than that of zinnwaldite in veinlet (309 m level). The REE content of all micas at different levels is low, most of which are under the detection limit. The micas show a geochemical variation for some elements with depth (Tables 1, 2; Fig. 9). The rare metal contents in micas generally increase trend with depth for W (from 5.5 to 94 ppm), Nb (from 0.20 to 145 ppm), Ta (from 0.01 to 182 ppm), Sn (from 61 to 777 ppm), Sc (from 6.3 to 241 ppm). But some elements in micas, such as MgO (from 5.48 to 0.01 wt %), Co (from 24.2 to 0.30 ppm), Ni (from 62.7 to 0.01 ppm), V (from 57.8 to 0.01 ppm), generally decrease with depth.

6.2 Wolframite

Chemical compositions of wolframite from different levels determined by EPMA and LA-ICP-MS are summarized in Table 3. MnO/FeO ratios of wolframite from greisen 0.74 to 1.08, while MnO/FeO ratios of wolframite from quartz veins and veinlets range from 0.63 to 3.82 (Fig. 10). The Fe/(Fe + Mn) ratios of wolframite in Maoping have two clusters. The Fe/(Fe + Mn) ratios of wolframite in 309 m (0.45–0.61), − 52 m (0.37–0.54) and greisen (0.48–0.57) are close to 0.5. But Wolframite from 40 m (0.29–0.38), − 5 m (0.21–0.24), − 30 m (0.22–0.31), − 75 m (0.21–0.31) and − 100 m (0.24–0.27) are close to the huebnerite endmember.

The wolframites show a geochemical variation for some elements with depth (Fig. 10). The rare metal contents in wolframite increase with depth for Nb (from 44.6 to 11,660 ppm), Ta (from 0.20 to 24,249 ppm), Sn (from 0.80 to 899 ppm), Mo (from 3.4 to 783 ppm). But some elements contents in wolframite decrease with depth for MgO (from 0.09 to 0.01 wt%), Co (from 4.5 to 0.01 ppm), V (from 9.1 to 0.01 ppm), Ti (from 551 to 1.3 ppm).

Wolframites in greisen and quartz vein display similar chondrite-normalized REE (REE_N) patterns (HREE-enriched) (Fig. 11). Wolframite in greisen has significantly negative Eu anomalies (δEu: average 0.001) (Table 3), whereas wolframite in quartz vein shows relatively weak negative Eu anomalies (δEu = 0.001–0.095, average = 0.016). wolframites in the veinlet (309 m level) even show positive Eu

Table 2 Summary of LA-ICP-MS analyses of micas from the Maoping deposit

	309 m		40 m	− 5 m	− 30 m	− 52 m	− 75 m	− 100 m	Greisen		Granite	
	Fe-rich phengite Mean (n = 11)	Fe-poor phengite Mean (n = 7)	Zinnwaldite Mean (n = 15)	Zinnwaldite Mean (n = 13)	Zinnwaldite Mean (n = 5)	Zinnwaldite Mean (n = 7)	Zinnwaldite Mean (n = 39)	Zinnwaldite Mean (n = 9)	Zinnwaldite Mean (n = 7)	Li phengite Mean (n = 11)	Protolithionite Mean (n = 5)	Li phengite Mean (n = 17)
Li_2O (wt%)	1.37	0.91	2.48	2.54	2.83	2.91	2.61	2.90	2.40	1.28	1.50	1.01
Be	20.4	22.5	12.1	13.1	14.4	15.5	17.5	14.2	9.5	14.5	11.9	15.4
B	9.8	21.9	7.8	10.9	7.7	8.7	6.9	7.3	9.9	26.7	11.3	27.0
Sc	9.7	10.3	14.1	17.3	35	26.4	23.8	32	26.1	30	175.3	100
V	33	36	14.2	2.85	0.48	1.92	3.25	2.57	0.65	0.68	2.55	1.43
Co	15.6	10.4	5.8	3.07	0.94	1.65	1.56	2.08	1.29	0.85	0.97	0.74
Ni	34	19.2	6.8	1.47	0.18	1.50	0.76	2.28	0.20	0.15	1.32	1.06
Zn	708	351	767	1307	1828	1664	1933	1876	1401	960	1171	853
Rb	6868	4676	8704	7128	9195	8523	7147	8501	8245	4751	7983	5966
Sr	0.63	6.1	0.59	0.36	0.10	0.14	0.26	0.20	0.10	0.18	0.83	0.74
Nb	0.75	2.64	5.4	9.9	24.1	6.0	17.5	19.9	96	42	114	77
Mo	0.24	0.17	0.78	0.98	1.29	1.18	1.53	0.99	0.38	0.68	0.13	0.07
Sn	121	177	215	232	313	242	271	255	555	518	549	544
Cs	449	317	523	476	609	546	523	532	543	155	579	340
Ba	180	777	136	35	3.0	17.3	27	24	7.7	5.6	2.2	2.9
Ta	0.0	0.1	1.9	17.1	19.8	1.1	12.5	18.2	153	45	96	53
W	7.3	9.5	22.6	25.1	44	33	30	39	51	85	57	50
Cr	1.4	4.8	1.7	0.2	0.9	0.3	6.5	1.4	2.5	2.4	1.2	2.3
Cu	2.01	3.63	0.96	6.0	3.44	2.89	0.39	1.80	0.72	0.78	0.20	0.52
Ga	101	65	133	97	119	109	96	104	141	158	124	115
Ge	9.5	8.0	9.0	9.3	8.8	9.9	8.9	10.9	11.1	10.1	8.8	8.9
In	0.54	0.82	3.4	2.60	4.6	3.8	3.5	3.7	8.6	10.4	6.9	6.9
Tl	32	23	37	32	34	33	30	32	32	17	31	23
Pb	3.4	5.3	4.7	4.6	5.0	4.3	4.2	4.7	5.9	8.8	5.5	6.4

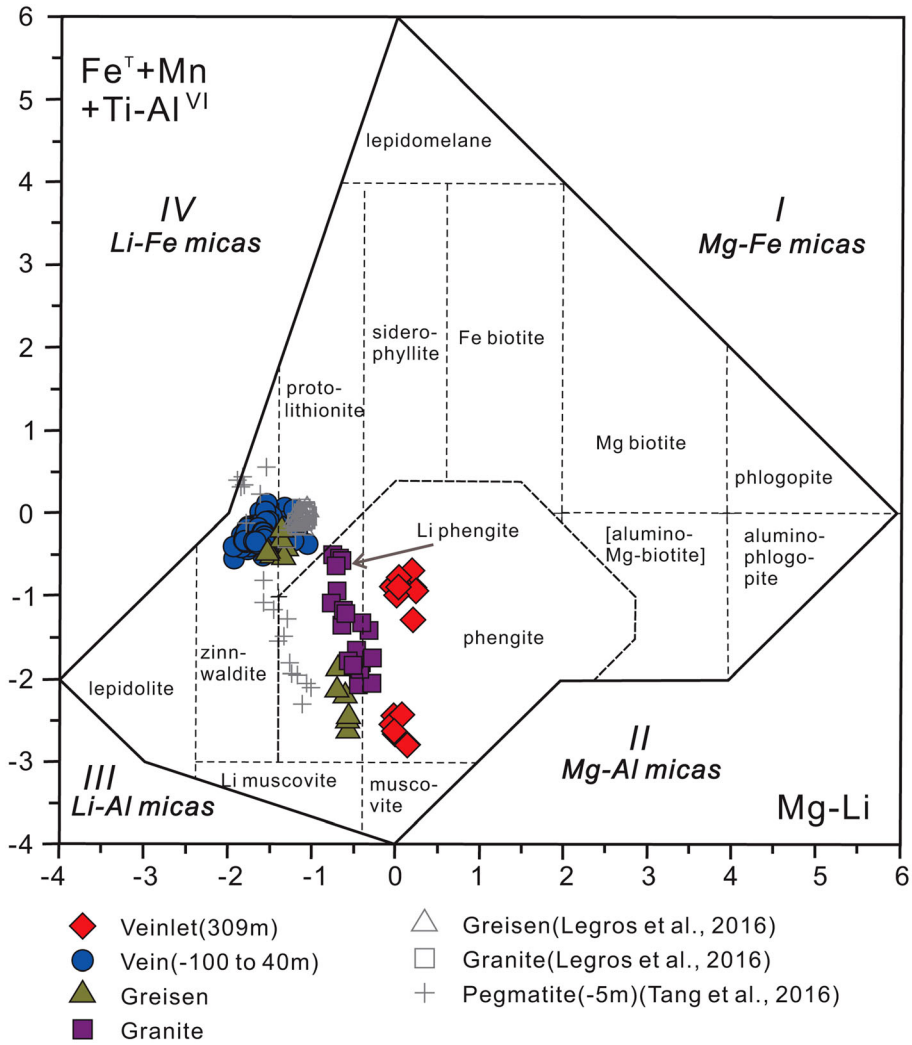

Fig. 8 Compositions of micas showed in the Tischendorf et al. (1997) discrimination diagram of Fe + Mn + Ti–Al VI versus Mg–Li

anomalies (δEu: 0.23–6.41, average 1.27) (Fig. 11h). Besides, the content of REE of wolframite in greisen (average ∑REE = 2523 ppm) is much higher than wolframite in quartz veins (average ∑REE = 210 ppm). Wolframite in quartz veinlets of 309 m level has the lowest ∑REE with an average of 12.7 ppm. On the whole, the content of the REE of wolframite increases gradually with depth.

Some wolframite grains of greisen is inhomogeneous. The CL-dark wolframite has lower REE (∑REE = 1900 ppm) and higher Nb (5899 ppm) and Ta (8194 ppm) than the CL-light zone (∑REE = 2372 ppm, Nb = 4033 ppm, Ta = 5481 ppm).

7 Discussion

7.1 Magmatic origin of ore-forming fluids

Micas and wolframite are common minerals in tungsten deposits. The compositions, especially the trace elements, can trace the source of fluids from which they precipitate. Zinnwaldites in greisen, have high W, Sn, Nb, Ta, similar as protolithionite in granite (Table 2; Fig. 9), which indicates that the zinnwaldite in greisen is of magmatic hydrothermal origin. Although micas in wolframite–quartz veins have highly variable W, Sn, Nb, and Ta, most micas, particularly micas at deep levels (< −50 m), have high W, Sn, Nb, and Ta. Nb and Ta are commonly enriched in high-temperature fluids and decrease with temperature decline (Liu and Cao 1987). High contents of Nb and Ta in wolframite possibly indicate that ore-forming fluids were originated from granitic magma (Harlaux et al. 2018). Therefore, ore-forming fluids are likely to be enriched in rare metals (such as W, Sn, Nb, Ta, etc.), supporting that the ore-forming fluids are dominated by magmatic-hydrothermal fluids.

Micas have very low REE contents so that REE patterns of hydrothermal micas cannot be used to trace the source of ore-forming fluids. Heavy REEs (HREEs) have ionic radii closer to Fe^{2+} and Mn^{2+} than light REEs (LREEs)

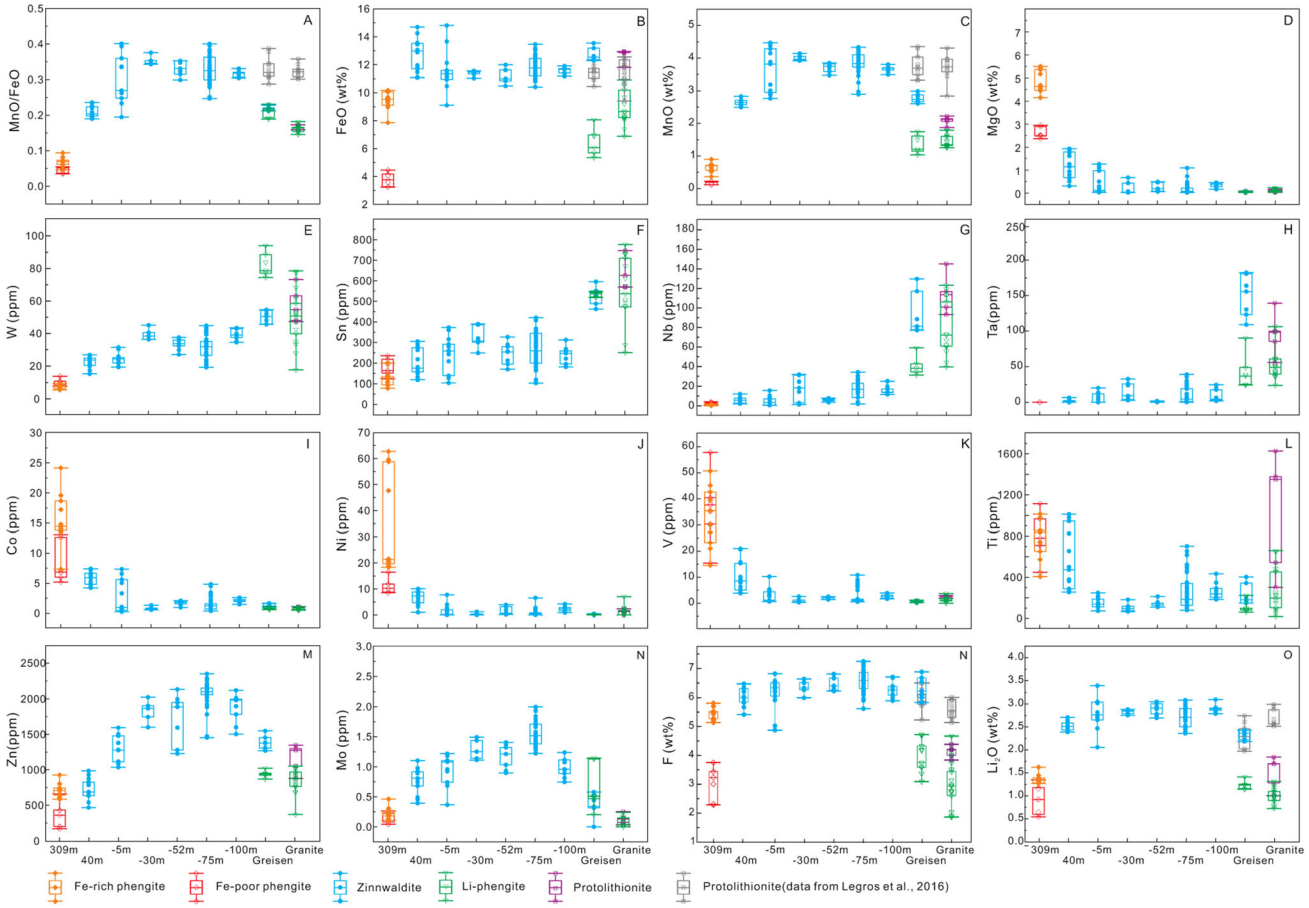

Fig. 9 Variation diagram of major and trace elements of mica in different levels of the Maoping deposit

(Shannon 1976). Thus, the partition coefficient between wolframite and ore-forming fluids of HREE would be much larger than those of LREE. Due to the lack of a partition coefficient of each element in wolframite, REE patterns of wolframite could not be directly used to constrain the REE composition of fluids. Wolframite grains in quartz-veins have similar REE patterns to those in greisen at the Maoping deposit (Fig. 12), showing the deletion of LREE and significantly negative Eu anomalies. The unique REE patterns, together with elevated Nb and Ta contents, indicate that wolframite in Maoping have a similar origin as those from the Xihuashan and Piaotang W deposits (Zhang et al. 2018), but different from those of low-temperature Woxi Au–Sb–W deposit (Zhu et al. 2014), indicative of the high-temperature magma-derived origin. Although wolframite in greisen and wolframite–quartz vein and veinlet have different REE concentrations and show different LREE-depleted REE_N patterns, they both have significantly negative Eu anomalies, similar to those of the granite (Fig. 11). Thus, negative Eu anomalies of the wolframite are likely inherited from the highly fractionated granite (c.f. Zhang et al. 2018).

Chen et al. (2018) reported oxygen isotope compositions of quartz and wolframite in the Maoping W deposit. Quartz in wolframite–quartz veins of zone III, IV and V (corresponding to the levels < -50 m) in Maoping has $\delta^{18}O$ values from 12.0 to 14.3 ‰, corresponding to the $\delta^{18}O$ values of ore-forming fluids of 5.0 to 7.2 ‰ (Chen et al. 2018). In contrast, wolframite has $\delta^{18}O$ values range from 4.1 to 6.0 ‰, corresponding to the $\delta^{18}O$ values of ore-forming fluid from 6.1 to 8.0 ‰. Both wolframite and quartz have oxygen isotopic compositions plotted in the magmatic water field, also support the magmatic origin for ore-forming fluids.

7.2 Evolution of ore-forming fluids and possible controls

Tungsten and Sn in mica and Sn in wolframite show continuously decreasing trend from the deep to shallow (Figs. 9, 10). Due to a lack of partition coefficient of W and Sn between mica and hydrothermal fluids, variations of contents of W and Sn in mica are assumed to represent the changing of W and Sn in ore-forming fluids. Precipitation

Table 3 Summary of major and trace elements of wolframite from the Maoping W deposit

	309 m Mean (n = 32)	40 m Mean (n = 8)	− 5 m Mean (n = 7)	− 30 m Mean (n = 16)	− 52 m Mean (n = 8)	− 75 m Mean (n = 47)	− 100 m Mean (n = 12)	Greisen Mean (n = 12)
Major elements (wt%)								
TiO_2	0.04	0.03	0.04	0.02	0.03	0.02	0.02	0.00
MgO	0.05	0.03	0.01	0.01	0.04	0.02	0.02	0.01
SnO_2	0.02	0.02	0.05	0.02	0.01	0.02	0.02	0.12
Sc_2O_3	0.03	0.05	0.02	0.07	0.01	0.06	0.04	0.03
FeO	14.1	7.9	5.3	6.3	11.6	6.1	6.0	12.6
WO_3	75.4	75.7	76.0	75.3	75.7	75.2	75.4	73.2
MnO	10.5	15.5	18.3	17.3	12.0	18.2	17.6	12.2
Ta_2O_5	0.11	0.05	0.18	0.29	0.05	0.21	0.17	0.94
Nb_2O_5	0.11	0.17	0.15	0.45	0.17	0.42	0.37	1.07
CaO	0.02	0.02	0.01	0.02	0.02	0.02	0.02	0.01
Total	100.2	99.5	99.8	99.7	99.6	100.2	99.6	100.2
Trace element (ppm)								
Sc	92	67	154	336	59	272	281	54
Ti	153	31	6.9	13.1	31	12.1	14.1	16.8
V	4.5	0.65	0.13	0.07	1.22	0.10	0.15	0.2
Co	3.2	0.55	0.23	0.12	0.97	0.15	0.20	0.5
Ni	0.9	0.17	0.06	0.04	0.55	0.05	0.06	0.0
Zn	75	160	176	177	117	166	182	158
Nb	576	890	570	3161	967	2640	2732	5180
Mo	14	29	21	58	104	41	66	500
Sn	8	12	16	153	10	90	75	256
La	0.01	0.01	0.01	0.03	0.01	0.06	0.01	0.1
Ce	0.01	0.04	0.08	0.37	0.15	0.27	0.20	1.0
Pr	0.003	0.02	0.04	0.18	0.08	0.10	0.10	0.5
Nd	0.02	0.22	0.42	1.97	0.74	1.01	1.13	5.3
Sm	0.06	0.91	1.83	6.24	2.62	3.44	4.19	16.7
Eu	0.03	0.03	0.01	0.01	0.05	0.02	0.01	0.1
Gd	0.15	2.02	3.8	13.3	6.5	7.1	9.4	46
Tb	0.10	1.26	2.21	6.7	3.8	3.9	4.8	25
Dy	1.29	15.5	25.1	74.6	46	40	55	296
Ho	0.38	3.8	5.7	16.3	11.2	9.4	12.2	83
Er	1.87	18.8	26.8	71.8	52.7	38.9	53.6	372
Tm	0.57	5.6	7.4	18.3	14.3	10.6	13.9	98
Yb	6.96	65	81	187	152	114	146	1022
Lu	1.25	10.4	12.3	27.2	23.2	17.3	21.7	168
Hf	0.26	0.75	1.25	11.6	1.01	5.3	4.0	22.6
Ta	12.78	378	503	2379	441	1316	1280	7687
Zr	7.58	8.0	13.7	61	9.1	50.3	32	132
U	1.80	2.75	5.3	32.1	3.6	29.2	23.4	56

of wolframite suggests that W is saturated in ore-forming fluids so that W contents in mica could be used as an indicator for the solubility of W in fluids.

Tungsten is thought to be transported in hydrothermal fluids as WO_4^{2-}, which is complexed with Na^+, K^+, Li^+, and H^+ (Wood and Samson 2000). Micas from greisen to 40 m mining level have nearly constant Li_2O (Fig. 9) suggesting that destablitiy of Li(Na)–W complex does not play an important role in decreasing the solubility of W in fluids. Thus, the solubility of W in hydrothermal fluids is

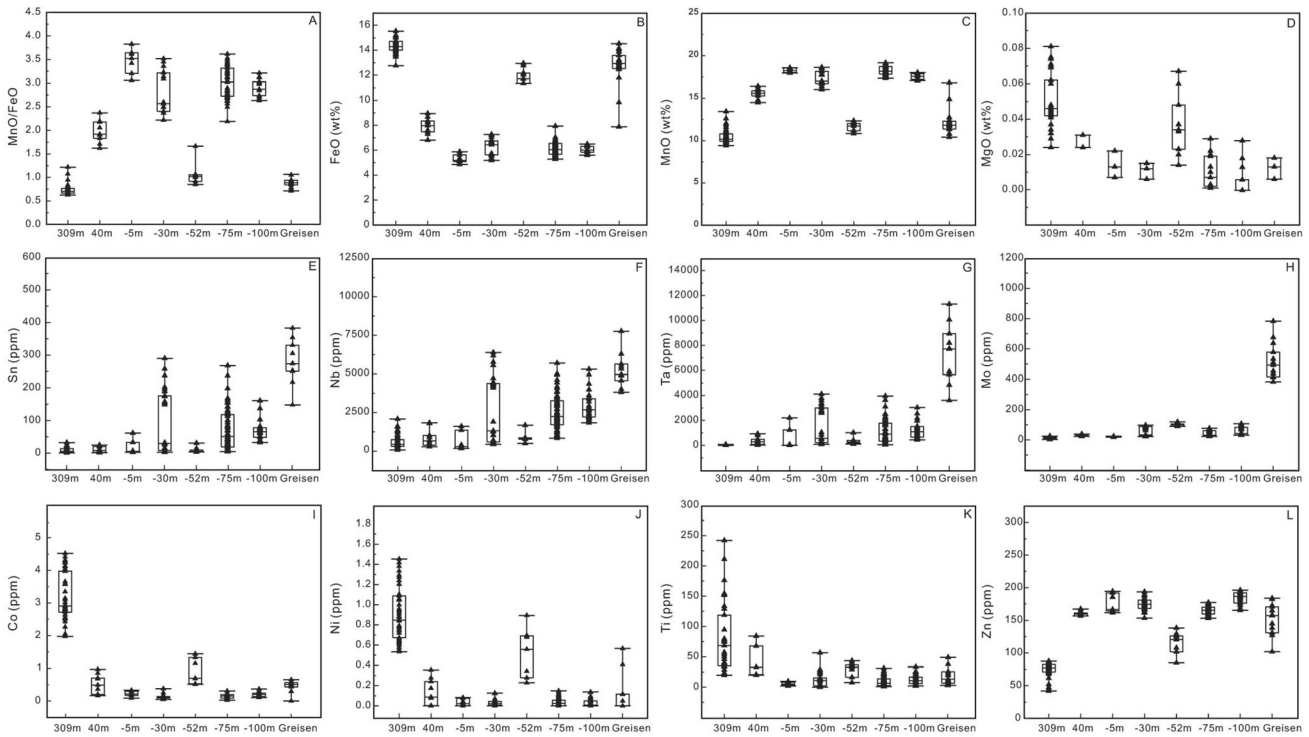

Fig. 10 Variation diagram of major and trace elements of wolframite in different levels of the Maoping deposit

mainly controlled by the pH values (Wood and Samson 2000) and temperature (Heinrich 1990; Wang et al. 2020). The loss of CO_2 could increase pH value of fluids and thus affect the transportation of W. CO_2-bearing fluid inclusions are commonly observed in quartz but rarely presented in wolframite, precluding the function of CO_2 in W transportation and deposition (Ni et al. 2015). In addition, the presence of muscovite in quartz-veins and nearly constant F contents in micas suggest that wolframite precipitation was not triggered by a strong increase of pH values (Michaud and Pichavant 2019). Thus, temperature decline is probably the main control of wolframite crystallization (c.f. Heinrich 1990).

Greisen is usually considered to be a product of high-T alteration (Pirajno 1992; Shcherba 1970). With the decreasing of temperature and pressure, the ore-forming fluids escape and fill the fractures in surrounding country rocks forming quartz-veins (Pirajno 2009). In Maoping, fluid inclusions in the wolframite–quartz vein are thought to show a slightly continuous decrease of homogenization temperature from deep to shallow (Chen et al. 2018). However, fluid inclusions in wolframite and quartz have similar homogenization temperature and salinity, suggesting that temperature variation of ore-forming fluids at these mining levels is not distinct. Both Nb and Ta are sensitive to temperature (Harlaux et al. 2018), wolframite and micas from − 100 to 40 m mining levels have similar Nb and Ta contents (Figs. 9, 10), supporting relatively constant temperature of fluids at such levels. Therefore, the decreasing temperature of fluids took place before the fluids enter the fractures where ore-forming fluids have a nearly constant temperature. In comparison, micas and wolframite from veinlets at 309 m level have the lowest Nb and Ta contents. Fluid inclusions in this level also have the lowest homogenization temperature, indicating the cooling of ore-forming fluids at a shallow level.

Wolframite from different levels of the Maoping deposit show a gradually decreasing trend in REE contents. Despite different REE concentrations of wolframite from variable levels, wolframite from the greisen, quartz vein and quartz veinlet have similar REE patterns. The previous study of wolframite from the Xihuashan and Piaotang deposits have shown that precipitation of wolframite would reduce the REE contents of the ore-forming fluid but would not change their REE patterns (Zhang et al. 2018). Therefore, the decrease of REE in wolframite in levels from the deep upwards indicates the evolvement of the ore-forming fluids. Europium has two different valences: 2 + and 3 +. The Eu^{3+} is easier to enter into wolframite lattice than Eu^{2+} according to the ionic radius so that the increase of oxygen fugacity would result in elevated Eu^{3+}/Eu^{2+} ratios in fluids and thus relatively high Eu_N/Eu^* ratios in wolframite. In the Maoping deposit, wolframites of both greisen and wolframite–quartz vein have the negative Eu anomalies, while wolframites in quartz veinlet from the 309 m level have positive Eu anomalies,

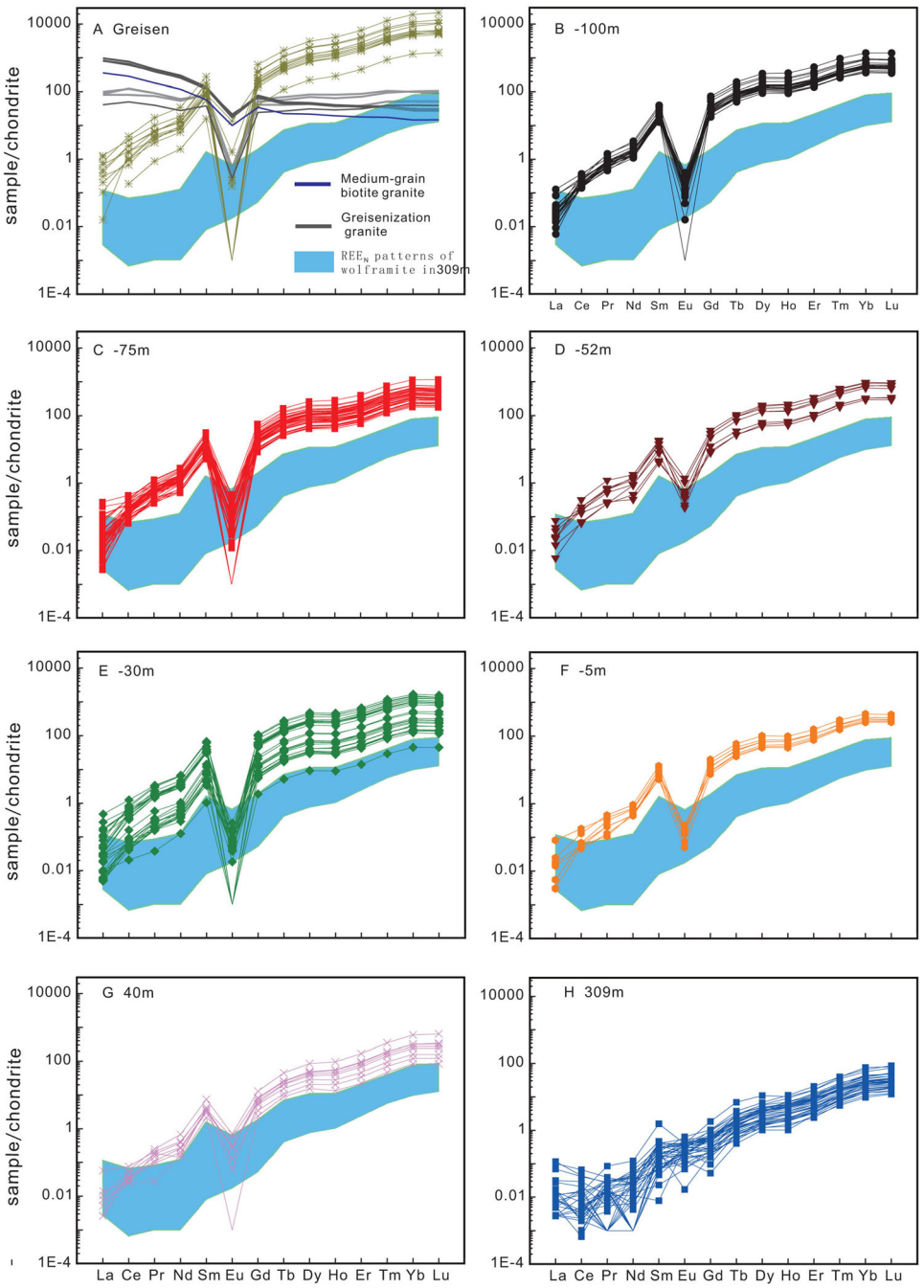

Fig. 11 REE patterns of wolframite in the Maoping deposits. REE values of chondrite are from Taylor and McLennan (1985); REE contents of the greisenized and medium-grain biotite granite in Maoping are from Zhu et al. (2012)

suggesting that fluids are relatively reduced in the deep (< 40 m level) but relatively oxidized at 309 m level. The negative Eu anomalies of wolframite in greisen may be inherited from the magma, while wolframite in quartz veinlets at 309 m level may indicate relatively the oxidized nature of ore-forming fluids. The drastic changing of oxygen fugacity might be caused by the addition of meteoric water in the shallow of the mineralization system, which is supported by the oxygen isotopes of wolframite and quartz (Chen et al. 2018). The similar variations of Eu anomalies in wolframite could be found in other tungsten deposits in Southern Jiangxi, such as Piaotang and Dawangshan (Lin 1988; Zhang et al. 2018), indicating that redox conditions of hydrothermal systems in the shallow level in the quartz-vein type tungsten mineralization would have been changed. The $Fe^{3+}/(Fe^{3+}+ Fe^{2+})$ ratio of mica can also record the variation of oxygen fugacity of fluids from which it precipitated (Li et al. 2013). From granite and greisen to the wolframite–quartz veins, $Fe^{3+}/(Fe^{3+}+ Fe^{2+})$ ratios show the slightly decreasing trend, suggesting that the oxygen fugacity of ore-forming fluids is slowly lowering. The relatively reduced nature of fluids

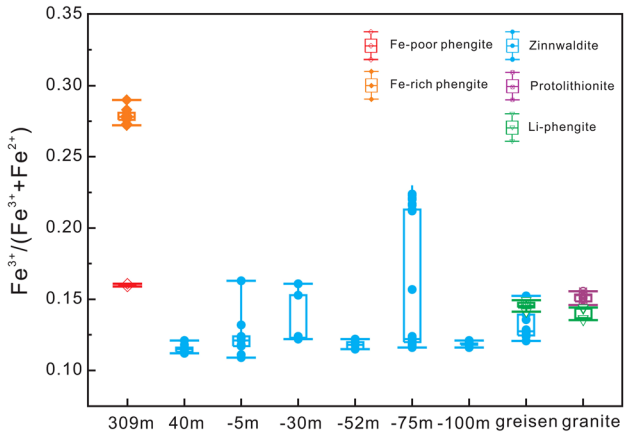

Fig. 12 Variation of Fe $^{3+}$/(Fe^{3+}+ Fe^{2+}) ratios of micas in different levels at the Maoping deposit

will be conducive to the formation of wolframite (Huang et al. 2014; Lecumberri-Sanchez et al. 2017; Li et al. 2013).

Different from W, Sn, Nb, Ta, and REEs, Zn is a chalcophile element and is sensitive to sulfide saturation. Sphalerite with economic value is mainly distributed in the quartz-veins in the Xiamaoping segment, with levels from ground to − 75 m (No. 2 team of Jiangxi Nonferrous Geological Prospecting 2010). The content of Zn in mica decreases from − 75 m, which is consistent with the precipitation of sphalerite from − 75 m (Fig. 9m), indicating that ore-forming fluids reach sulfide saturation at about − 75 m level. With the precipitation of sphalerite, the content of Zn in the fluid decreases gradually.

7.3 The possible role of fracture system in quartz-vein type mineralization

The wolframites in greisen often show the dark core and bright overgrowth in the BSE image. The Nb and Ta contents of the dark domain (Nb = 5900 ppm, Ta = 8190 ppm) are higher than the bright domain (Nb = 4030 ppm, Ta = 5480 ppm), indicating that the dark domain formed at a higher temperature than the bright domain. The bright overgrowth has Nb and Ta higher than wolframite in quartz veins. Thus, the dark domain is possible of magmatic origin, while the bright domain is produced by the early hydrothermal activity. During the emplacement of the magma and the interaction of rock and country rocks, the formation of the fracture system in upper strata would result in depressurization and vapor loss. Ore-forming fluids would fill the fractures quickly. The country rocks of upper strata have a lower temperature so that the heat exchange between the country rocks and fluids filling the fracture would lower the temperature of ore-forming fluids, triggering precipitation of wolframite.

Previous studies have shown that the existence of CO_2 could favor the transportation of tungsten (Higgins 1980; Wang et al. 2020; Wood and Samson 2000). The escape of CO_2 and the decrease of the pressure of ore-forming fluids would lead to precipitation of wolframite and quartz in the fracture system (Korges et al. 2018). The temperature of fluids in the deep level of the vein systems remains constant, suggesting that the formation of the fracture system and the filling of fluids in fractures are very quick. Due to the quick transportation, the ore-forming fluids do not have strong interaction with country rocks and only generate very thin alteration selvage (generally less than 2 km) along quartz veins. With the decrease of the flow rate of ore-forming fluids in the shallow, recycled meteoric water in strata has been added into the emplacing fluids and changing the temperature and oxygen fugacity of fluids.

In summary, the fracture system can highly affect the emplacement and evolution of ore-forming fluids, leading to the deposition of quartz, wolframite, mica, and sphalerite at different levels. Due to the fast flow rate, the interaction between hydrothermal fluids and country rocks are limited. The variation of the composition, oxygen fugacity of ore-forming fluids are mainly controlled by the precipitation of minerals in fracture system themselves.

8 Conclusions

1. In situ compositions of micas and wolframite from in situ analyses indicate that the ore-forming fluids in the Maoping deposit are mainly of magmatic origin.
2. Brittle fractures control the depressurization and fluid mixing of ore-forming fluids, leading to the wolframite mineralization.
3. The geochemical compositional variation as well as the physicochemical processes of the ore-forming fluids are mainly controlled by the deposition of micas and wolframite during the emplacement and evolution of fluids.

Acknowledgements This work is financially supported by the National Key R&D Program of China (2016YFC0600207), Key Program of Natural Science Foundation of China (41830428), and the "CAS Hundred Talents" Project to JF Gao. We are grateful to Dr. Juan Li at the School of Earth Sciences and Engineering, Nanjing University for taking BSE images. We also thank the staff of the Nanjing FocuMS Technology Co. Ltd. for their kind help in in situ LA-ICP-MS analysis. Finally, thanks for Helene Legros, Lili Chen, Guanglai Li, and Zeying Zhu's help and advice.

Author contributions All authors contributed to the conception and design study. Data collection and analysis: GHC and JFG; Methodology: JFG and JJL; Writing, original draft preparation: GHC; Writing, review and editing: JFG, JJL and RQZ. All authors read and approved the final manuscript.

References

Breiter K, Hložková M, Korbelová Z, Galiová MV (2019) Diversity of lithium mica compositions in mineralized granite–greisen system: Cínovec Li–Sn–W deposit, Erzgebirge. Ore Geol Rev 106:12–27. https://doi.org/10.1016/j.oregeorev.2019.01.013

Chen J, Jahn B-M (1998) Crustal evolution of southeastern China: Nd and Sr isotopic evidence. Tectonophysics 284:101–133. https://doi.org/10.1016/S0040-1951(97)00186-8

Chen L-L, Ni P, Li W-S, Ding J-Y, Pan J-Y, Wang G-G, Yang Y-L (2018) The link between fluid evolution and vertical zonation at the Maoping tungsten deposit, Southern Jiangxi, China: fluid inclusion and stable isotope evidence. J Geochem Explor 192:18–32. https://doi.org/10.1016/j.gexplo.2018.01.001

Feng C, Zeng Z, Zhang D, Qu W, Du A, Li D, She H (2011) SHRIMP zircon U-Pb and molybdenite Re–Os isotopic dating of the tungsten deposits in the Tianmenshan-Hongtaoling W–Sn ore-field, southern Jiangxi Province, China, and geological implications. Ore Geol Rev 43:8–25. https://doi.org/10.1016/j.oregeorev.2011.04.006

Gao J-F, Zhou M-F, Lightfoot PC, Wang CY, Qi L, Sun M (2013) Sulfide saturation and magma emplacement in the formation of the Permian Huangshandong Ni–Cu sulfide deposit, Xinjiang, Northwestern China. Econ Geol 108:1833–1848. https://doi.org/10.2113/econgeo.108.8.1833

Goldmann S, Melcher F, Gäbler H-E, Dewaele S, Clercq FD, Muchez P (2013) Mineralogy and trace element chemistry of ferberite/reinite from tungsten deposits in central Rwanda. Minerals 3:121–144

Harlaux M, Mercadier J, Marignac C, Peiffert C, Cloquet C, Cuney M (2018) Tracing metal sources in peribatholitic hydrothermal W deposits based on the chemical composition of wolframite: the example of the Variscan French Massif Central. Chem Geol 479:58–85. https://doi.org/10.1016/j.chemgeo.2017.12.029

Heinrich CA (1990) The chemistry of hydrothermal tin(-tungsten) ore deposition. Econ Geol 85:457–481. https://doi.org/10.2113/gsecongeo.85.3.457

Higgins NC (1980) Fluid inclusion evidence for the transport of tungsten by carbonate complexes in hydrothermal solutions. Can J Earth Sci 17:823–830. https://doi.org/10.1139/e80-082

Hu D-Q, Hua R-M, Li G-L, Wei X-L, Huang X-E (2011a) Study on the fluid inclusions of Maoping tungsten deposit, Southern Jiangxi Province. Geol J China Univ 17:327–336

Hu M-Y et al (2011b) Preliminary Characterisation of New Reference Materials for Microanalysis: Chinese Geological Standard Glasses CGSG-1, CGSG-2, CGSG-4 and CGSG-5. Geostand Geoanal Res 35:235–251. https://doi.org/10.1111/j.1751-908X.2010.00097.x

Huang DT (1999) Geological characteristics of Maoping tungsten-tin deposit. China Tungsten Ind 3:23–24

Huang F et al (2014) Genesis of the Yuanlingzhai porphyry molybdenum deposit, Jiangxi province, South China: Constraints from petrochemistry and geochronology. J Asian Earth Sci 79:759–776. https://doi.org/10.1016/j.jseaes.2013.05.016

Jiang G-H (2004) Chlorine and fluorine control on copper and tungsten mineralization in hydrothermal deposits—case of Dexing porphyry copper deposit and Dajishan tungsten deposit in Jiangxi Province. Institute of Geochemistry, Chinese Academy of Science

Korges M, Weis P, Lüders V, Laurent O (2018) Depressurization and boiling of a single magmatic fluid as a mechanism for tin-tungsten deposit formation. Geology 46:75–78. https://doi.org/10.1130/g39601.1

Lecumberri-Sanchez P, Vieira R, Heinrich CA, Pinto F, Wälle M (2017) Fluid–rock interaction is decisive for the formation of tungsten deposits. Geology 45:579–582. https://doi.org/10.1130/g38974.1

Legros H et al (2016) Detailed paragenesis and Li-mica compositions as recorders of the magmatic-hydrothermal evolution of the Maoping W–Sn deposit (Jiangxi, China). Lithos 264:108–124. https://doi.org/10.1016/j.lithos.2016.08.022

Legros H et al (2018) The ore-forming magmatic-hydrothermal system of the Piaotang W–Sn deposit (Jiangxi, China) as seen from Li-mica geochemistry. Am Miner 103:39–54

Li Y, Yang Y (1991) Basic geological characteristics of tungsten-tin deposit in Maoping, Jiangxi Province. Miner Resour Geol 04:186–204

Li X-H, Li Z-X, Li W-X, Liu Y, Yuan C, Wei G, Qi C (2007) U–Pb zircon, geochemical and Sr–Nd–Hf isotopic constraints on age and origin of Jurassic I- and A-type granites from central Guangdong, SE China: a major igneous event in response to foundering of a subducted flat-slab? Lithos 96:186–204. https://doi.org/10.1016/j.lithos.2006.09.018

Li J, Zhong J-W, Yu Y, Huang X-L (2013) Insights on magmatism and mineralization from micas in the Xihuashan granite, Jiangxi Province, South China. Geochimica 42:393–404

Li J, Liu Y, Zhao Z, Chou IM (2018) Roles of carbonate/CO2 in the formation of quartz-vein wolframite deposits: Insight from the crystallization experiments of huebnerite in alkali-carbonate aqueous solutions in a hydrothermal diamond-anvil cell. Ore Geol Rev 95:40–48. https://doi.org/10.1016/j.oregeorev.2018.02.024

Lin SW (1988) Rare earth elements in wolframite–quartz veins, Jiangxi. Geol Prospect 2:19–24

Liu YJ, Cao LM (1987) Introduction to elemental geochemistry. Geological Publishing House, Beijing

Liu Y, Hu Z, Gao S, Günther D, Xu J, Gao C, Chen H (2008) *In-situ* analysis of major and trace elements of anhydrous minerals by LA-ICP-MS without applying an internal standard. Chem Geol 257:34–43. https://doi.org/10.1016/j.chemgeo.2008.08.004

Mao J et al (2019) Geology and metallogeny of tungsten and tin deposits in China. In: Society of Economic Geologists Special Publication, vol 22, pp 411–482

Mao J, Cheng Y, Chen M, Franco P (2013) Major types and time–space distribution of Mesozoic ore deposits in South China and their geodynamic settings. Miner Depos 48:267–294. https://doi.org/10.1007/s00126-012-0446-z

Michaud JA-S, Pichavant M (2019) The H/F ratio as an indicator of contrasted wolframite deposition mechanisms. Ore Geol Rev 104:266–272. https://doi.org/10.1016/j.oregeorev.2018.10.015

Monier G, Robert J-L (1986) Evolution of the miscibility gap between muscovite and biotite solid solutions with increasing lithium content: an experimental study in the system K_2O–Li_2O–MgO–FeO–Al_2O_3–SiO_2–H_2O–HF at 600°C, 2 kbar P H_2O: comparison with natural lithium micas. Miner Mag 50:641–651. https://doi.org/10.1180/minmag.1986.050.358.09

Ni P, Wang X-D, Wang G-G, Huang J-B, Pan J-Y, Wang T-G (2015) An infrared microthermometric study of fluid inclusions in coexisting quartz and wolframite from Late Mesozoic tungsten deposits in the Gannan metallogenic belt, South China. Ore Geol Rev 65:1062–1077. https://doi.org/10.1016/j.oregeorev.2014.08.007

No. 2 team of Jiangxi Nonferrous Geological Prospecting (1989) Detailed Geological Survey Report of the Maoping W–Sn Deposite in Chongyi County, Jiangxi Province

No. 2 team of Jiangxi Nonferrous Geological Prospecting (2010) Checking Report on Resources and Reserves of Maoping Tungsten Mine in Chongyi County, Jiangxi Province

Pirajno F (1992) Greisen systems. In: Pirajno F (ed) Hydrothermal mineral deposits: principles and fundamental concepts for the

exploration geologist. Springer, Berlin, pp 280–324. https://doi.org/10.1007/978-3-642-75671-9_10
Pirajno F (2009) Hydrothermal processes and mineral systems. Springer, Berlin. https://doi.org/10.1007/978-1-4020-8613-7
Selby D, Creaser RA (2005) Direct radiometric dating of hydrocarbon deposits using rhenium–osmium isotopes. Science 308:1293–1295. https://doi.org/10.1126/science.1111081
Shannon R (1976) Revised effective ionic radii and systematic studies of interatomic distances in halides and chalcogenides. Acta Crystallogr A 32:751–767. https://doi.org/10.1107/S0567739476001551
Shcherba GN (1970) Greisens. Int Geol Rev 12:114–150. https://doi.org/10.1080/00206817009475216
Shu LS, Zhou XM, Deng P, Yu XQ (2006) Principal geological features of Nanling tectonic belt, South China. Geol Rev 52:251–265
Shui T (1988) Tectonic framework of the continental basement of southeastern China. Sci China B 31:885–896
Tang A, Li GL, Zhou LQ, Su Y, Tong KY (2016) Geological characteristics of micas with zonal structure in pegmatite from maoping tungsten deposit and its significance to magma-fluid evolution process, Southern Jiangxi. Geol Sci Technol Inf 1:30–37
Taylor SR, McLennan SM (1985) The continental crust: its composition and evolution. Blackwell Scientific Publications, Oxford
Tindle AG, Breaks FW (2000) Columbite-tantalite mineral chemistry from rare-element granitic pegmatites: separation Lakeh area, N.W. Ontario, Canada. Miner Petrol 70:165–198. https://doi.org/10.1007/s007100070002
Tindle AG, Webb PC (1990) Estimation of lithium contents in trioctahedral micas using microprobe data: application to micas from granitic rocks. Eur J Mineral 2:595–610
Tischendorf G, Gottesmann B, Forster H-J, Trumbull RB (1997) On Li-bearing micas: estimating Li from electron microprobe analyses and an improved diagram for graphical representation. Miner Mag 61:809–834
Wang X-L et al (2007) Detrital zircon geochronology of Precambrian basement sequences in the Jiangnan orogen: dating the assembly of the Yangtze and Cathaysia Blocks. Precambr Res 159:117–131. https://doi.org/10.1016/j.precamres.2007.06.005
Wang X et al (2020) *In-situ* Raman spectroscopic investigation of the hydrothermal speciation of tungsten: implications for the ore-forming process. Chem Geol 532:119299. https://doi.org/10.1016/j.chemgeo.2019.119299
Wei W, Hu R, Bi X, Peng J, Su W, Song S, Shi S (2012) Infrared microthermometric and stable isotopic study of fluid inclusions in wolframite at the Xihuashan tungsten deposit, Jiangxi province, China. Miner Depos 47:589–605. https://doi.org/10.1007/s00126-011-0377-0
Wood SA, Samson IM (2000) The hydrothermal geochemistry of tungsten in granitoid environments: I. relative solubilities of ferberite and scheelite as a function of T, P, pH, and mNaCl. Econ Geol 95:143–182. https://doi.org/10.2113/gsecongeo.95.1.143
Xia Y, Xu X, Niu Y, Liu L (2018) Neoproterozoic amalgamation between Yangtze and Cathaysia blocks: the magmatism in various tectonic settings and continent-arc-continent collision. Precambr Res 309:56–87. https://doi.org/10.1016/j.precamres.2017.02.020
Xie L, Wang Z, Wang R, Zhu J, Che X, Gao J, Zhao X (2018) Mineralogical constraints on the genesis of W–Nb–Ta mineralization in the Laiziling granite (Xianghualing district, south China). Ore Geol Rev 95:695–712. https://doi.org/10.1016/j.oregeorev.2018.03.021
Yuan S, Williams-Jones AE, Mao J, Zhao P, Yan C, Zhang D (2018) The origin of the Zhangjialong tungsten deposit, South China: implications for W–Sn mineralization in large granite batholiths. Econ Geol 113:1193–1208. https://doi.org/10.5382/econgeo.2018.4587
Zeng Z-L, Zhu X-P, Xu J-X (2007) Tungsten reserves of Southern Jiangxi Province and prospecting outlook. China Tungsten Ind 6:16–18
Zhang Q, Zhang R-Q, Gao J-F, Lu J-J, Wu J-W (2018) *In-situ* LA-ICP-MS trace element analyses of scheelite and wolframite: constraints on the genesis of veinlet-disseminated and vein-type tungsten deposits, South China. Ore Geol Rev 99:166–179. https://doi.org/10.1016/j.oregeorev.2018.06.004
Zhao J-H, Zhou M-F, Yan D-P, Zheng J-P, Li J-W (2011) Reappraisal of the ages of Neoproterozoic strata in South China: no connection with the Grenvillian orogeny. Geology 39:299–302. https://doi.org/10.1130/g31701.1
Zhou XM, Li WX (2000) Origin of Late Mesozoic igneous rocks in Southeastern China: implications for lithosphere subduction and underplating of mafic magmas. Tectonophysics 326:269–287. https://doi.org/10.1016/S0040-1951(00)00120-7
Zhou XM, Sun T, Shen WZ, Shu LS, Niu YL (2006) Petrogenesis of Mesozoic granitoids and volcanic rocks in South China: a response to tectonic evolution. Episodes 29:26–33
Zhu MB, Tang HY, He DH, Li HZ (2012) Geochemical characteristics of Maoping tungsten-tin deposit granite in Jiangxi Province. Nonferrous Met (Min Sect) 64:34–39
Zhu YN, Peng JT, Liu SY, Sun YZ (2014) Mineral deposit geology and trace element geochemistry of wolframite from the Woxi deposit, western Hunan, China. Geochimica 43:287–300